The asymmetric Ekman decay of cyclonic and anticyclonic vortices

Luis Zavala Sansón [1]

Fluid Dynamics Laboratory, Department of Physics, Eindhoven University of Technology, Eindhoven, The Netherlands

Abstract – Recent studies have shown differences in the behaviour of cyclonic and anticyclonic quasi-two-dimensional vortices in laboratory experiments in a rotating fluid. In this paper, the role of dissipative effects due to bottom topography is investigated as a possible cause for the asymmetry in the spin-down of both types of vortices. The basic mechanism of Ekman friction in 2D mathematical models is the presence of a linear damping term in the vorticity equation, which produces the flow decay. Here, an extended 2D formulation including nonlinear Ekman corrections is considered. The aim is to show that nonlinear Ekman effects are responsible for the different decay of cyclonic and anticyclonic vortices, while the conventional formulation (only containing the linear friction term) predicts a symmetric decay for both cases.

In order to illustrate the role of nonlinear Ekman effects, axisymmetric vortices are simulated numerically. The relatively simple structure of such vortices allows a better understanding of their evolution. The main difference in the spin-down process of cyclones and anticyclones is the decay rate, which is faster for cyclonic motion. Furthermore, it is shown that the basic mechanism for such a difference is the outward advection of fluid in cyclones and inward in anticyclones, both effects due to Ekman pumping and suction, respectively. The results derived here intend to provide a physical interpretation which could be applied for more general, non-axisymmetric structures. © 2001 Éditions scientifiques et médicales Elsevier SAS

1. Introduction

In large-scale geophysical flows, such as the oceans or the atmosphere, the Earth's rotation plays a fundamental role. A remarkable characteristic frequently observed in these flows is the emergence of quasi-2D coherent structures, e.g., tropical cyclones in the atmosphere or warm and cold eddies in the oceans. These vortices are predominantly two-dimensional (2D), i.e. parallel to a plane tangent to the Earth's surface and perpendicular to the local component of the planet's angular velocity. The basic 2D motion of monopolar and dipolar vortices in the presence of background rotation is also observed in laboratory experiments, e.g., in a rotating fluid tank (see Hopfinger and van Heijst [1]). Although there are important differences with geophysical flows, the laboratory experiments are a useful tool for understanding the basic behaviour of large-scale vortices affected by the planet's rotation.

In laboratory experiments with density-homogeneous vortices, some fundamental differences are often observed between cyclonic (rotating in the same direction as the tank) and anticyclonic vortices. For instance, Kloosterziel and van Heijst [2] have shown the behaviour of different types of cyclones, which approximately remain 2D (i.e. the fluid moves in columns aligned with the axis of rotation) for long periods of time, compared with the rotation period of the tank. In contrast, anticyclonic vortices usually present a more complicated evolution, which in some cases may lead to the vortex cleavage or to 3D turbulent motion (Kloosterziel and van Heijst [3]). Apparently, only very weak anticyclones are able to remain coherent (see also Maas [4]; Sipp et al. [5]).

*E-mail address:* lzavala@cicese.mx (L. Zavala Sansón).

[1] Present address: Department of Physical Oceanography, CICESE, Ensenada, Baja California, México.

In this paper, the role of dissipative effects due to bottom topography is investigated as a possible cause for the asymmetry in the spin-down of both types of vortices. Although such effects are usually very weak, they may be crucial on the long-term evolution of quasi-2D flows affected by rotation. In other words, only the slow viscous decay of circular vortices will be studied, without considering in detail their stability or instability properties.

Viscous effects associated with bottom topography can be derived by applying linear Ekman theory inside the boundary layer (the so-called Ekman layer) at the no-slip bottom, which is usually very thin compared with the total fluid depth. The influence of bottom friction in the (interior) 2D flow is given by the exchange of fluid with the Ekman layer, as shown in *figure 1*, where a sketch of the so-called 'Ekman condition' is presented (see, e.g., Gill [6]). When the interior flow has positive relative vorticity (ω) with respect to the angular velocity (Ω) of the rotating system, there is pumping of fluid from the Ekman layer towards the interior, thus squeezing fluid columns. On the other hand, when the interior flow has negative relative vorticity, there is suction of fluid towards the Ekman layer, thereby stretching the flow.

Taking advantage of the predominantly 2D motion in rotating fluid systems, bottom friction can be incorporated in 2D mathematical formulations and solved numerically. This simplification will be used in this paper. In conventional theory, the inclusion of bottom friction consists of adding a linear term in the vorticity equation (see, e.g., Pedlosky [7]). As a result, the interior relative vorticity of cyclones decays exponentially at the same rate as anticyclones (with initial oppositely signed vorticity distribution). In other words, the conventional formulation with Ekman damping does not distinguish between cyclonic and anticyclonic vortices. It was recently shown by Zavala Sansón and van Heijst [8] (henceforth ZSvH), however, that weak nonlinear Ekman friction terms can be incorporated in a 2D model with a flat bottom and solved numerically. These terms, although rather small, lead to significant differences compared with the conventional approximation when studying the evolution of experimental barotropic cyclones. Also, the asymmetric decay between cyclones and anticyclones is observed when using this formulation in numerical simulations of dipolar vortices on a flat bottom (Zavala Sansón et al. [9]). This study is aimed at providing a physical interpretation of nonlinear Ekman effects on the asymmetric decay of cyclonic and anticyclonic vortices.

In order to illustrate the differences between cyclonic and anticyclonic motion affected by bottom friction, non-isolated axisymmetric vortices will be considered. There are two reasons for using these simplified structures. On one hand, they remain nearly axisymmetric during the decay process. The relatively simple
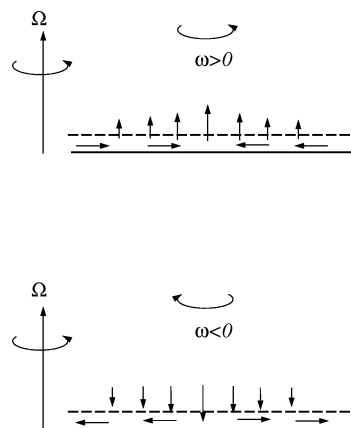
Figure 1. Influence of the Ekman layer in the 2D interior flow with relative vorticity ω: for $\omega > 0$ (upper sketch) there is pumping of fluid towards the interior, while for $\omega < 0$ (lower sketch) there is suction from the interior flow to the Ekman layer.

structure of such vortices therefore allows a better understanding of the numerical results obtained from simulations based on the 2D viscous model with nonlinear Ekman effects. In contrast, isolated vortices develop instabilities that result in the formation of multipolar vortices (see, e.g., van Heijst et al. [10]; Orlandi and Carnevale [11]). On the other hand, non-isolated cyclonic vortices are easily reproduced in laboratory experiments (see, e.g., Kloosterziel [2]; ZSvH [8]), i.e. they are physically realistic. Although there are no equivalent anticyclonic vortices observed in laboratory experiments, they will also be numerically simulated here in order to illustrate the difference with cyclonic vortices. The obtained results intend to provide a physical interpretation which could be used to explain such a difference for more general structures, namely non-axisymmetric vortices.

The rest of the paper is organized as follows. In section 2 the viscous extended model including nonlinear Ekman effects is presented. Numerical simulations, based on the 2D model, of cyclonic and anticyclonic axisymmetric vortices are presented in section 3. The results are extensively discussed in section 4, and summarized in section 5.

2. Basic equations

2.1. Viscous model

In this section, the quasi-two-dimensional model with Ekman friction derived by ZSvH [8] is presented. This model applies to a homogeneous fluid layer over a flat horizontal surface, rotating at a constant angular speed. The upper free surface is assumed to be flat and with no friction. Using conventional Cartesian coordinates (x, y, z), the angular rotation $\mathbf{\Omega} = (0, 0, \Omega)$ is taken anti-parallel to the gravitational acceleration $\mathbf{g} = (0, 0, -g)$. The evolution equation in the vorticity-stream function formulation is

$$\frac{\partial \omega}{\partial t} + J(\omega, \psi) - \frac{1}{2}E^{1/2}\nabla\psi \cdot \nabla\omega = \nu\nabla^2\omega - \frac{1}{2}E^{1/2}\omega(\omega + f), \tag{1}$$

where $\omega = \partial v/\partial x - \partial u/\partial y$ is the z component of the relative vorticity, (u, v) are the velocity components in the (x, y) directions, respectively, t is the time, ν is the kinematic viscosity, $f = 2\Omega$ is the Coriolis parameter, $\nabla^2 = \partial^2/\partial x^2 + \partial^2/\partial y^2$ is the horizontal Laplacian operator, J is the Jacobian operator, and E is the Ekman number defined by

$$E = \frac{2\nu}{fH^2}, \tag{2}$$

where H is the fluid depth. The terms proportional to $E^{1/2}$, which is much smaller than unity, represent the bottom friction effects. The (nonlinear) Ekman terms in the left-hand side of (1) are the corrections to the advective terms $J(\omega, \psi)$ due to bottom friction. The Ekman terms in the right-hand side represent stretching effects associated with the Ekman pumping. The stream function ψ is related to the relative vorticity through the Poisson equation

$$\omega = -\nabla^2\psi, \tag{3}$$

and the horizontal velocities are

$$u = \frac{\partial \psi}{\partial y} - \frac{1}{2}E^{1/2}\frac{\partial \psi}{\partial x}, \tag{4}$$

$$v = -\frac{\partial \psi}{\partial x} - \frac{1}{2}E^{1/2}\frac{\partial \psi}{\partial y}. \tag{5}$$

The conventional 2D model including bottom damping only considers the linear part of the Ekman stretching terms in the vorticity equation:

$$\frac{\partial \omega}{\partial t} + J(\omega, \psi) = \nu \nabla^2 \omega - \frac{1}{2} E^{1/2} f \omega. \tag{6}$$

Under this approximation, the stream function and the vorticity are related through the Poisson equation (3), but the horizontal velocities do not include the correction $O(E^{1/2})$ as in (4) and (5).

Both formulations (1) and (6) are based on the linear Ekman condition, which yields an expression for the vertical velocity, w, produced by the thin Ekman layer at the flat bottom:

$$w|_{z=\delta_E} = \frac{1}{2} \delta_E \omega \tag{7}$$

(see, e.g., Gill [6]; Pedlosky [7]), where $\delta_E = (2\nu/f)^{1/2}$ is the thickness of the bottom Ekman layer. Note that the vertical velocity is proportional to the relative vorticity of the interior flow outside the Ekman layer and, therefore, it implies pumping (suction) of fluid for cyclonic (anticyclonic) vortices, as shown in *figure 1*. Although the Ekman condition (7) is valid only for low Rossby number flow, model (1) provides a good description of the decay of intense vortices in laboratory experiments, as found by ZSvH. The simulations presented here include both weak and strong vortices.

The basic mechanism of Ekman friction in models (1) and (6) is the presence of the linear term $(-\frac{1}{2} E^{1/2} f \omega)$, which produces an exponential decay in the relative vorticity. When only considering this linear damping effect, the vorticity equation (6) is invariant to changes $\{\omega\} \to \{-\omega\}$, implying that cyclonic vortices decay at the same rate as anticyclones. This model therefore is not able to predict asymmetries between both types of vortices. The nonlinear terms, in contrast, are responsible for the differences between cyclones and anticyclones, as will be shown in the rest of the paper.

2.2. Vorticity equation in cylindrical coordinates

Consider the azimuthal component of the 2D Navier–Stokes equation, written in cylindrical coordinates (r, θ, z), while assuming axisymmetric flow $(\partial/\partial\theta = 0)$

$$\frac{\mathrm{D} v_\theta}{\mathrm{D} t} + f u_r + \frac{u_r v_\theta}{r} = \nu \frac{\partial}{\partial r} \left(\frac{1}{r} \frac{\partial (r v_\theta)}{\partial r} \right), \tag{8}$$

where (u_r, v_θ) are the radial and azimuthal velocities, respectively, and the material derivative is

$$\frac{\mathrm{D}}{\mathrm{D} t} = \frac{\partial}{\partial t} + u_r \frac{\partial}{\partial r} \tag{9}$$

(see, e.g., Maas [4]). Defining the relative vorticity ω as

$$\omega = \frac{1}{r} \frac{\partial}{\partial r} (r v_\theta), \tag{10}$$

equation (8) transforms into

$$\frac{\partial v_\theta}{\partial t} + u_r(\omega + f) = \nu \frac{\partial \omega}{\partial r}. \tag{11}$$

When the linear Ekman condition is considered, it is found that the weak radial velocity is proportional to the azimuthal velocity

$$u_r = \frac{1}{2} E^{1/2} v_\theta, \tag{12}$$

as noted by, e.g., Kloosterziel and van Heijst [2] and Maas [4]. This result, together with (10) and (11), yields the vorticity equation:

$$\frac{\partial \omega}{\partial t} + \frac{1}{2} E^{1/2} v_\theta \frac{\partial \omega}{\partial r} = \nu \frac{1}{r} \frac{\partial}{\partial r} \left(r \frac{\partial \omega}{\partial r} \right) - \frac{1}{2} E^{1/2} \omega(\omega + f) \tag{13}$$

(see also ZSvH [8]). Note that the only advective term in the left-hand side of this equation is associated with nonlinear Ekman effects, since the Jacobian term in (1) vanishes for axisymmetric flows.

3. Evolution of axisymmetric vortices

3.1. Radial profiles

In order to illustrate the differences between cyclones and anticylones affected by bottom friction, a well-known axisymmetric vortex frequently observed in laboratory experiments will be considered. The so-called 'sink vortex' (see, e.g., Kloosterziel and van Heijst [2,3]; ZSvH [8]) is a cyclonic vortex created in rotating tank experiments by locally syphoning a fixed amount of fluid, during a certain period of time, through a thin perforated tube. The sink vortices have a single-signed vorticity and are hence non-isolated. Cyclonic sink vortices are remarkably stable (Kloosterziel and van Heijst [2,3]) and they remain nearly axisymmetric during the decay process. For the flat-bottom case, typical radial distributions of the vorticity and azimuthal velocity are

$$\omega_{\text{sink}}(r) = \omega_0 \exp\left(\frac{-r^2}{R^2} \right), \tag{14}$$

$$v_{\text{sink}}(r) = \frac{R^2 \omega_0}{2r} \left[1 - \exp\left(\frac{-r^2}{R^2} \right) \right], \tag{15}$$

where ω_0 is the peak vorticity, R a horizontal length scale, and r the radial distance to the centre of the vortex. The Rossby number, measuring the strength of the vortex with respect to the background rotation, can be defined as $\varepsilon = \omega_0/f$. Although there are no equivalent anticyclonic vortices observed in laboratory experiments, a 'sink' anticyclone (defined by $-\omega_0$, with $\omega_0 > 0$) will be numerically simulated here in order to illustrate the differences with cyclonic vortices.

The decay of cyclonic sink vortices in laboratory experiments was recently studied in detail by ZSvH [8]. The basic quantities measured in the experiments and simulations were the radius of maximum velocity ($R_{\max}$), the maximum velocity ($V_{\max}$) and the peak vorticity in the vortex core (ω_0). These authors showed that the decay process (measured by observing the temporal evolution of these parameters) is well predicted in numerical simulations when nonlinear Ekman terms are taken into account. A similar procedure is followed here, but now comparing numerical simulations of cyclonic and anticyclonic vortices. The method for calculating the vortex parameters consists of fitting the numerical results of the vorticity field to expression (14), in order to obtain R and ω_0. The parameters $R_{\max}$ and $V_{\max}$ are directly measured from the obtained velocity profile. An additional

quantity calculated in this paper is the total kinetic energy defined as

$$K = \frac{1}{2} \iint (u^2 + v^2) \, dx \, dy. \tag{16}$$

The numerical simulations of ZSvH [8] also showed the outward spiral motion of a passive tracer in a cyclonic vortex, due to nonlinear Ekman effects. It will be shown in this study, that fluid is advected inward in anticyclones, as expected.

3.2. The numerical parameters

The numerical simulations were performed by means of a finite differences code used in ZSvH [8]. The numerical domain is a rectangle of $L_x \times L_y = 100 \times 100$ cm with no-slip boundaries, which is discretized by 128×128 grid points; a constant time step $\delta t = 0.1$ s was used in all simulations; the Coriolis parameter is taken 1 s^{-1}, the kinematic viscosity is 0.01 cm^2 s^{-1}, and the fluid depth is 18 cm (these numerical values were chosen corresponding to the laboratory arrangement in ZSvH, except the domain size; in that study a rectangle of 150×100 cm was used). The duration of the simulations is of order T_E, the Ekman time scale, defined as

$$T_E = \frac{2}{f E^{1/2}} = \left(\frac{2}{f \nu} \right)^{1/2} H. \tag{17}$$

For such times, bottom friction effects became manifest. The Ekman time scale is usually much longer than the rotation period of the system. For instance, under typical experimental conditions $E \approx 10^{-4}$, and therefore $T_E \approx 255$ s, while the rotation period of the system is $2\pi/(f/2) \approx 12.5$ s.

Typical vortex parameters in laboratory experiments are $\omega_0 \approx 3$ to 5 s^{-1} and $R \approx 2$ to 4 cm. These values correspond with initially intense vortices (i.e. with $\varepsilon \approx O(1)$). Here, the simulations are performed for both weak and strong vortices. As will be shown, weak and intense cyclones behave in a similar way, while weak and strong anticyclones present some important differences. The vortex parameters are chosen $\omega_0 = \pm 1$ s^{-1} and $R = 2.86$ cm for weak vortices and $\omega_0 = \pm 3.26$ s^{-1} and $R = 2.86$ cm for intense vortices. In all simulations the vortex was placed at the centre of the domain.

Although cyclonic sink vortices in laboratory experiments are usually intense, their behaviour is well predicted by the extended 2D model (1) (see ZSvH [8]). Unfortunately, it is extremely difficult to obtain stable, intense anticyclonic structures in the laboratory (see Kloosterziel and van Heijst [3]), and thereby a similar study has not been made. Even so, strong anticyclonic vortices are numerically simulated here in order to illustrate the differences with cyclonic vortices. Furthermore, the results indicate a possible mechanism causing the characteristic unstable behaviour of anticyclones (see the discussion section).

3.3. Advection effects in axisymmetric vortices

When the bottom Ekman condition is considered for axisymmetric vortices it is found that the azimuthal and radial velocities are related by (12). Rewriting this equation as

$$\frac{dr}{dt} = \frac{1}{2} E^{1/2} r \frac{d\theta}{dt}, \tag{18}$$

an expression for the radial position r of a fluid parcel as a function of the angular coordinate θ can be found:

$$r = r_0 \exp\left[\frac{1}{2}E^{1/2}(\theta - \theta_0)\right]. \tag{19}$$

This is the equation for a spiral when θ increases (cyclonic motion) or decreases (anticyclonic motion) monotonically. According to (19), the radial position of fluid columns in a cyclonic vortex increases in each turn, i.e. they are advected outward. In contrast, fluid parcels in an anticyclonic vortex are advected inward. This difference between both types of vortices leads to the asymmetry in their viscous decay, as will be discussed below.

The spiral motion of passive tracers within cyclones and anticyclones is shown by means of numerical simulations based on the viscous model (1). This behaviour is shown in *figure 2*, where the calculated trajectories of a passive tracer in the weak cyclone and anticyclone are plotted. In both cases the particle is initially placed at $(x_0, y_0) = (R, 0)$. The tracer moves in a spiral trajectory, outward for the cyclonic vortex and inward for the anticyclone, as predicted by (19). The outward advection of fluid in a cyclonic vortex was also shown by ZSvH [8]. In *figure 2*, the radial distance of the particle from the circle of radius x_0 and its angular component as a function of time are also presented. Since the decay is slower in the anticyclone and the tracer moves in an inward trajectory, it performs more revolutions than in the cyclonic case. It has to be recalled that
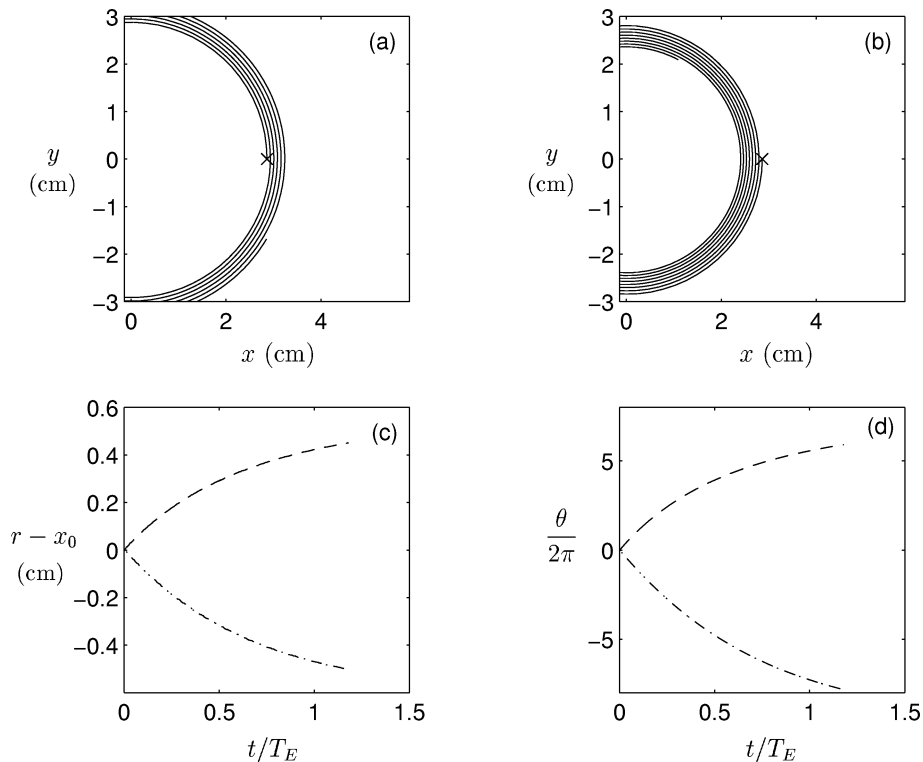
Figure 2. Upper row: calculated trajectories of a passive tracer in the weak cyclone (a) and anticyclone (b). The initial vortex parameters are $\omega_0 = \pm 1$ s^{-1} and $R = 2.86$ cm. The initial position of the tracer ($\times$) is $(x_0, y_0) = (R, 0)$. Lower row: (c) time evolution of the radial distance of the tracer from the circle of radius x_0 in the cyclone $(- - -)$ and the anticyclone $(- \cdot - \cdot -)$; (d) time evolution of the corresponding angular coordinate of the tracer in both simulations.
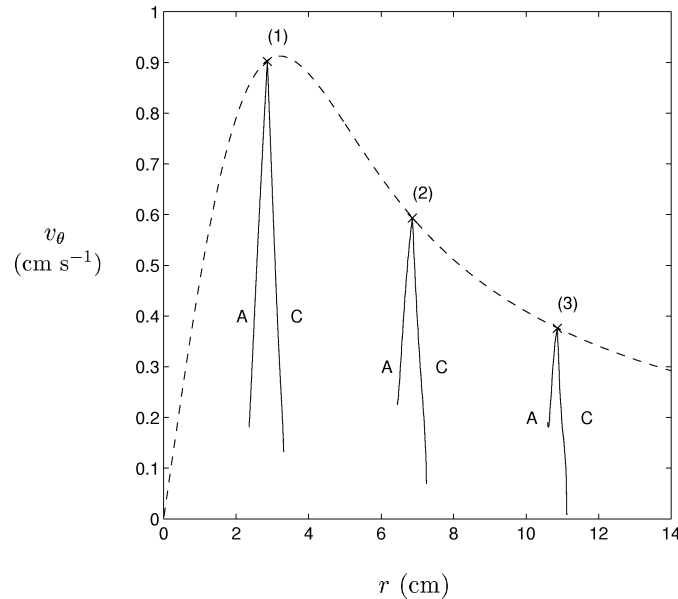
Figure 3. Numerically calculated azimuthal velocities (in absolute value) as a function of r of three particles in the weak cyclone (C) and anticyclone (A). The tracers are initially placed at a different radius: $r_{01} = R$, $r_{02} = 2.4R$, $r_{03} = 3.8R$. The initial velocity profile is also shown (dashed line).

in the absence of nonlinear Ekman effects, there is no radial advection of fluid and, therefore, the material trajectories are circles (see ZSvH [8]).

In *figure 3* the calculated azimuthal velocities of three passive tracers initially placed at a different radial position are shown. For the anticyclone, the particle velocities are calculated in absolute value in order to compare with the cyclonic case. It can be observed that both in the cyclone and in the anticyclone, the particle velocity is reduced as it moves outward or inward, respectively. Such a decrease is not symmetric, however, as the figure clearly shows. The azimuthal velocity of the three particles decreases faster in the cyclone.

3.4. Evolution of radial profiles

Sink vortices remain nearly axisymmetric during the decay process. Their initial parameters, therefore, can be considered as functions of time. *Figure 4* shows the evolution of the vortex parameters (R_{max}, V_{max}, K and ω_0) measured in the numerical simulations of a weak cyclonic and anticyclonic vortex. Absolute values of V_{max} and ω_0 for the anticyclone are plotted in order to make a direct comparison with the cyclone.

In *figure 4a* it is observed that the radius of maximum velocity of both vortices is increased. The expansion of the cyclonic vortex is associated with two mechanisms, namely lateral viscous effects (Kloosterziel [12]) and nonlinear Ekman effects (Kloosterziel and van Heijst [2]; Maas [4]; ZSvH [8]). Due to the Ekman condition at the bottom for cyclonic motion, the vertical velocity induced by the Ekman layer is positive (upwards), hence giving rise to an expansion of the vortex. For anticyclones, in contrast, lateral friction and nonlinear Ekman effects are counteracted, because the Ekman condition implies a negative vertical velocity induced by the Ekman layer, and therefore a contraction of the vortex. The radius of maximum velocity of the weak anticyclone, however, still increases in time, which indicates that lateral friction dominates this process. This is also inferred from the fact that R_{max} increases faster for the cyclone than for the anticyclone. *Figures 4b, 4c* and *4d* show that the decay of maximum velocity V_{max}, kinetic energy K and peak vorticity ω_0 is faster for the cyclonic case.
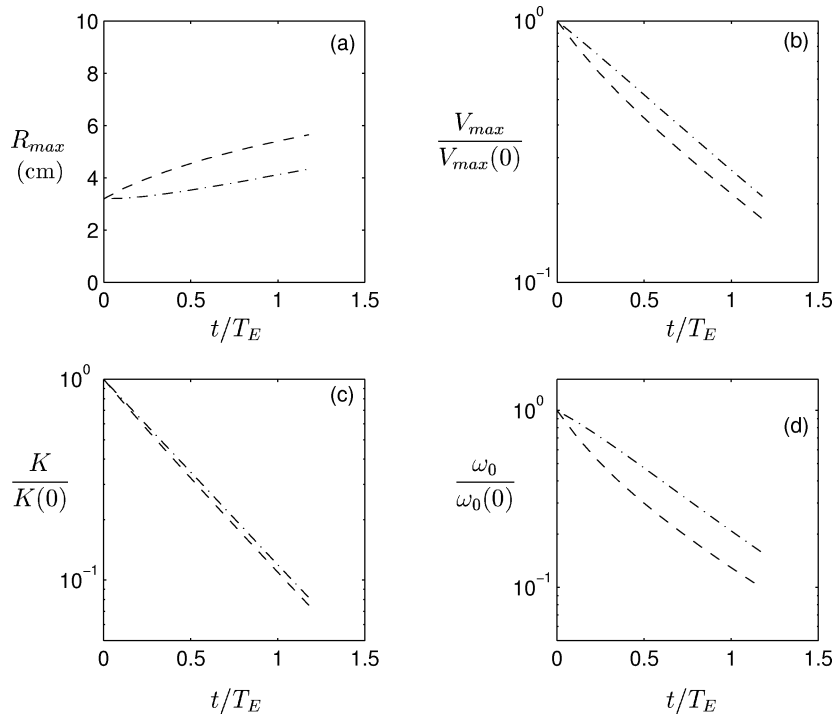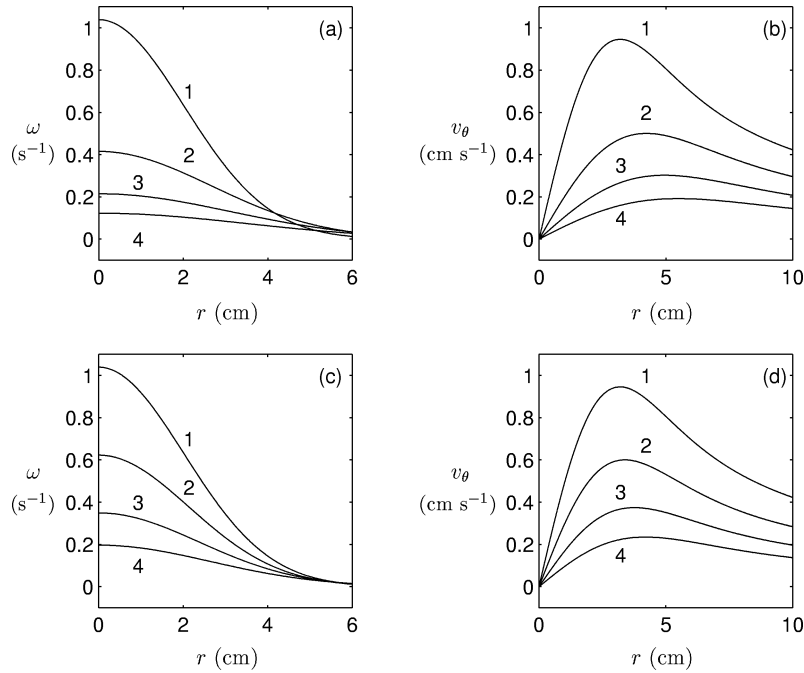
Figure 4. Time evolution of the weak cyclonic $(- - -)$ and anticyclonic $(- \cdot - \cdot -)$ vortex parameters: (a) radius of maximum velocity $(R_{\max})$; (b) maximum velocity $(V_{\max})$; (c) total kinetic energy (K), and (d) peak vorticity (ω_0). The parameters $V_{\max}$ and ω_0 corresponding to the anticyclone are shown in absolute value.

Since the vortex parameters are measured as a function of time, the evolution of the vorticity and velocity radial profiles can be obtained. These profiles are shown in *figure 5* for the cyclone ((a), (b)), and for the anticyclone ((c), (d)) at four different times. The expansion of both vortices is clearly observed, as well as the faster decay of the cyclonic vortex.

Additional simulations with strong vortices have been performed. *Figure 6* shows the evolution of the vortex parameters measured in the numerical simulations of intense cyclonic and anticyclonic vortices. In *figure 6(a)* it is observed that the radius of maximum velocity in the cyclonic case increases, while it is reduced for the anticyclone at the beginning of the simulation, although weakly increases at later stages. As in the weak cyclone, the increase of $R_{\max}$ in the strong vortex is the result of both lateral and (nonlinear) bottom friction. In the strong anticyclone these effects are opposed and, in contrast with the weak vortex, nonlinear effects dominate at early stages in the simulation. As the vortex decays, however, these effects are reduced and lateral friction produces the increase of $R_{\max}$ at later times.

Figures 6(b) and *6(c)* show that the decay of the maximum velocity $V_{\max}$ and kinetic energy K is faster for the cyclonic case. The peak vorticity in the anticyclonic vortex, however (see *figure 6(d)*), increases at initial times while decreasing at later stages. This behaviour is only observed in simulations with strong anticyclones, and is related with the sign of the absolute vorticity $\omega + f$, as will be discussed in the last section. Taking into account the initial contraction of the vortex, this result could be intuitively expected.
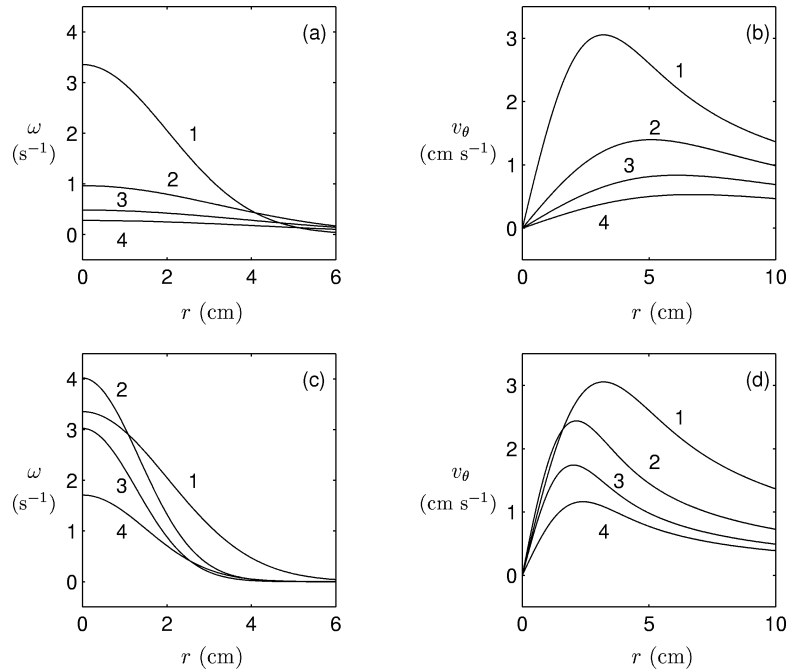
The corresponding evolution of the radial profiles at four different times are plotted in *figure 7*. The expansion of the cyclone is clearly observed, while the anticyclone is contracted first ($R_{\max}$ decreases and ω_0 increases) and later is slowly expanded.

Figure 5. Time evolution of the vorticity (a) and velocity (b) radial profiles of the weak cyclonic vortex. The corresponding profiles for the weak anticyclone are shown in absolute value in (c) and (d). The profiles are calculated by using the vortex parameters at (1) 0, (2) $0.35T_E$, (3) $0.7T_E$ and (4) $1.05T_E$, where $T_E = 255$ s.
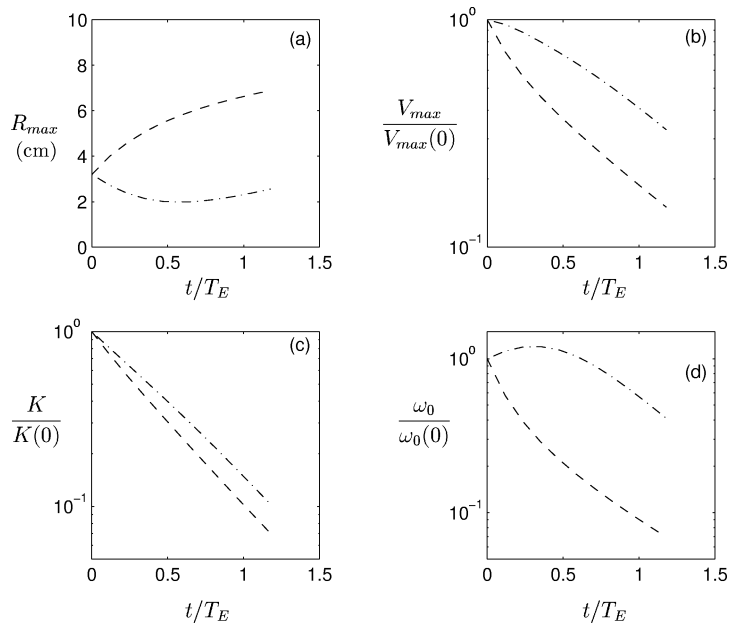
Figure 6. Time evolution of the strong cyclonic $(- - -)$ and anticyclonic $(- \cdot - \cdot -\cdot)$ vortex parameters: (a) radius of maximum velocity (R_{max}); (b) maximum velocity (V_{max}); (c) total kinetic energy (K), and (d) peak vorticity (ω_0). The initial vortex parameters are $\omega_0 = \pm 3.26$ s^{-1} and $R = 2.86$ cm. The parameters V_{max} and ω_0 corresponding to the anticyclone are shown in absolute value.

Figure 7. Time evolution of the vorticity (a) and velocity (b) radial profiles of the strong cyclonic vortex. The corresponding profiles for the strong anticyclone are shown in absolute value in (c) and (d). The profiles are calculated by using the vortex parameters at (1) 0, (2) $0.35T_E$, (3) $0.7T_E$ and (4) $1.05T_E$, where $T_E = 255$ s.

4. Discussion

Due to nonlinear Ekman effects two main differences have been found between cyclones and anticyclones: (i) cyclonic vortices decay faster than anticyclones, and (ii) fluid is radially advected in a spiral fashion, outward in cyclones and inward in anticyclones. In addition, the following results on the evolution of both types of vortices were observed. Weak and intense cyclonic vortices were observed to expand (increase of the radius of maximum velocity R_{max}), while decaying (decrease of V_{max}, K and ω_0). The same tendency was observed for weak anticyclones, but at a slower rate. For the case of strong anticyclonic vortices a decrease of the radius of maximum velocity, R_{max}, and an increase of the peak vorticity, ω_0, were observed at initial stages of motion. At later times, however, the expansion and decay of these two parameters, respectively, was found.

A physical interpretation for all these observations, based on the role of nonlinear Ekman effects, is proposed here. First, the radial advection of fluid is easily explained by considering the Ekman condition: fluid is pumped from the Ekman layer into cyclonic vortices, thus producing the radially outward advection; the opposite process occurs in anticyclones, where there is suction from the vortex into the boundary layer, therefore inducing the inward advection of fluid. Both features are remarkably captured by the simple 2D viscous model (1), as shown in *figure 2*. In ZSvH it was found that fluid particles remain at the same circular orbit when nonlinear Ekman effects are not taken into account in the numerical simulations (i.e. based on the conventional model (6)).

On the other hand, the faster decay of cyclones has been found and reported before in several studies, although a clear physical interpretation has not been provided. Here it is proposed that this behaviour is a consequence of an inviscid process driven by the radial advection of fluid. In order to show this, consider the

inviscid form of the azimuthal component of the 2D Navier–Stokes equation (8):

$$\frac{\mathrm{D}v_\theta}{\mathrm{D}t} + fu_r + \frac{u_r v_\theta}{r} = 0. \tag{20}$$

This expression implies the material conservation of the absolute angular momentum (see Kloosterziel and van Heijst [3])

$$\frac{\mathrm{D}}{\mathrm{D}t}\left(v_\theta r + \frac{1}{2}fr^2\right) = 0. \tag{21}$$

In absence of the Ekman layer (and assuming that the circular shape of the vortex is preserved), fluid particles remain at the same radial position and therefore their velocities also remain constant. In the present case, however, the nonlinear Ekman effects force the fluid to move radially outward (cyclones) or inward (anticyclones). How does this motion affect the particle velocity? The absolute angular momentum of a particle i can be written as

$$c_i = v_i r_i + \frac{1}{2}fr_i^2, \tag{22}$$

where v_i and r_i are its azimuthal velocity and radial position, respectively. Since c_i is conserved, it can be expressed as $c_i = v_{i0}r_{i0} + \frac{1}{2}fr_{i0}^2$, with the subindex 0 indicating the velocity and position at $t = 0$. Considering that a small change in radial position, Δr, implies an increment in the velocity, Δv, the conservation law can be written as

$$v_{i0}r_{i0} + \frac{1}{2}fr_{i0}^2 = (v_{i0} + \Delta v)(r_{i0} + \Delta r) + \frac{1}{2}f(r_{i0} + \Delta r)^2. \tag{23}$$

Neglecting quadratic terms, this expression is reduced to

$$\Delta v = -\frac{\Delta r}{r_{i0}}(fr_{i0} + v_{i0}). \tag{24}$$

Two situations have to be considered:

$$\text{(a)} \quad fr_{i0} + v_{i0} > 0, \tag{25}$$

$$\text{(b)} \quad fr_{i0} + v_{i0} < 0. \tag{26}$$

Case (a). The first condition, (25), is satisfied by any particle in a weak cyclone ($v_{i0} > 0$) or anticyclone ($-v_{i0} < 0$). For cyclonic vortices the Ekman layer produces an increase of the radial position ($\Delta r > 0$). This implies $\Delta v < 0$, i.e. the azimuthal velocity of a particle at any initial radius is reduced as it moves outwards. The Ekman layer produces a decreasing radial position ($\Delta r < 0$) in anticyclonic vortices, which yields $\Delta v > 0$. Therefore, the azimuthal velocity ($-v_{i0} + \Delta v$) is also reduced. Assuming that the particle experiences the same displacement in radial direction in both vortices, it is verified that

$$\left|\frac{\Delta v_A}{\Delta v_C}\right| = \frac{fr_{i0} - v_{i0}}{fr_{i0} + v_{i0}} < 1, \tag{27}$$

i.e. the decrease of the azimuthal velocity in the cyclone (C) is larger than in the anticyclone (A). It is concluded therefore that the radial displacement induces a larger decay in the azimuthal velocity of cyclonic particles than in anticyclones. This behaviour was observed in *figure 3*. Note that this change of velocity is only due to the change in radial position (which was driven by the Ekman condition).
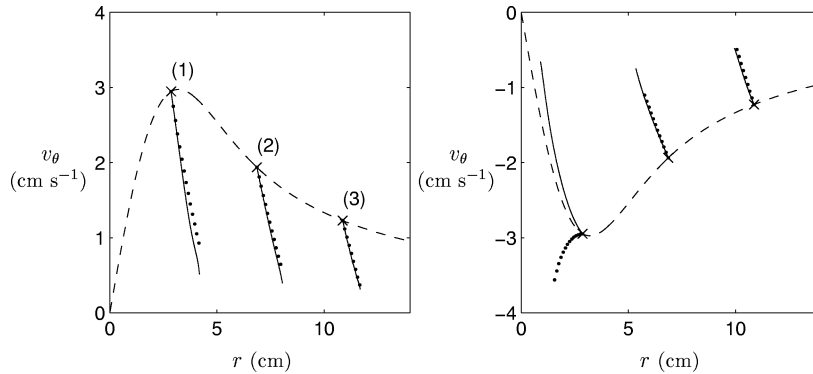
Figure 8. (a) Numerically calculated azimuthal velocities as a function of r of three particles in the strong cyclone (solid lines). The tracers are initially placed at a different radius: $r_{01} = R$, $r_{02} = 2.4R$, $r_{03} = 3.8R$. In addition, the azimuthal velocities calculated according with conservation of absolute angular momentum, (22), are also shown (dotted lines). (b) Same as in (a) but now for the strong anticyclonic vortex.

Any particle in a strong cyclonic vortex also satisfies the condition (25), and thus a decrease in the azimuthal velocity will also be observed (Δr is positive). This is shown in *figure 8(a)* where the velocities of three particles in a strong sink vortex according to (22), with r_i an increasing variable, are shown (dotted lines). The particles are initially at a different radius and they move outward a distance comparable to that in the numerical simulations. The corresponding velocities calculated from the simulation are also shown (solid lines). Note that the decay in the simulation is slightly faster, due to the presence of lateral friction.

Case (b). Strong anticyclones are a special case, since particles initially placed far from the peak velocity satisfy (25), otherwise they satisfy (26). The first situation implies a decrease of the azimuthal velocity, as in previous situations. In the second case, i.e. a particle in an intense anticyclone close to the peak value, the velocity may be intensified. Both situations are shown in *figure 8(b)* for the case of the strong anticyclonic vortex. When the initial velocity of the particle is far from the peak value, the azimuthal velocity decreases as the particle moves inward. In contrast, when the particle is placed initially close to the radius of maximum velocity, its velocity increases. This example shows that strong anticyclones are potentially unstable, as usually found in laboratory experiments. In the simulation, of course, the presence of diffusive effects prevent the increase of the azimuthal velocity, and therefore a decay is also observed (solid line).

4.1. Energy decay

In order to illustrate these results in terms of energy, consider again the motion equation for the azimuthal velocity (20), without lateral friction. Using the definition for the relative vorticity (10) and the Ekman condition (12) yields

$$\frac{\partial v_\theta}{\partial t} + \frac{1}{2} E^{1/2} v_\theta (\omega + f) = 0. \tag{28}$$

Multiplying by v_θ and defining the kinetic energy measured at a radius r as

$$K_r(r, t) = \frac{1}{2} v_\theta^2(r, t), \tag{29}$$

yields

$$\frac{\partial K_r}{\partial t} + E^{1/2} K_r (\omega + f) = 0. \tag{30}$$

This equation illustrates the different effects induced by the Ekman layer on cyclonic and anticyclonic vortices.

- First, note that for $|\omega| \ll f$ an equation for the total kinetic energy K can be obtained (by integrating over the whole domain), whose solutions are $K = K(0) \exp(-t/T_E)$. Therefore the kinetic energy decays at the same rate in both types of vortices, as expected.
- When the absolute vorticity at a certain radius is positive ($\omega + f > 0$) there is a decrease of the kinetic energy K_r. This is the case for any cyclonic vortex (arbitrary $\omega > 0$) or weak anticyclones (small $\omega < 0$). This loss, however, is larger for cyclones than for anticyclones. As explained before, such a difference arises from the outward (inward) motion of fluid in cyclones (anticyclones).
- In contrast, when the absolute vorticity is negative ($\omega + f < 0$), which is the case of intense anticyclones, the kinetic energy may be increased.

In the latter case, the increase of kinetic energy is, of course, inhibited by diffusive effects and the linear Ekman decay, always present in the numerical simulations. In other words, the net result of the linear viscous effects (lateral friction and linear Ekman effects) is a decrease of energy, while nonlinear Ekman effects play a different role depending on the sign of the absolute vorticity: they reinforce the decay when $\omega + f > 0$ (an effect which is stronger in cyclones than in anticyclones), but they reduce it for $\omega + f < 0$.

4.2. Peak vorticity

The peak vorticity evolution in the present simulations can be explained by using similar arguments. In the centre of the vortex, the vorticity equation (13) without lateral friction can be written as

$$\frac{\partial \omega_0}{\partial t} + \frac{1}{2} E^{1/2} \omega_0 (\omega_0 + f) = 0, \tag{31}$$

where ω_0 is the peak vorticity. Note that the advective Ekman correction is zero at $r = 0$. Again, for arbitrary cyclones and weak anticyclones (such that $\omega_0 + f > 0$) the peak vorticity decays, while for strong anticyclones ($\omega_0 + f < 0$) increases. Also, cyclonic peak vorticities decay faster.

All these situations are confirmed by *figures 4* and *6*. In particular, the increase of the peak vorticity in the strong anticyclone can be observed in *figure 6(d)*. At later stages, however, the peak vorticity decreases. This behaviour is easily explained by considering again that linear dissipative effects (lateral and linear Ekman friction) are continuously producing the vortex decay, and therefore weakening the role of the nonlinear (and linear) Ekman terms. Physically, the Ekman suction is reduced as the anticyclone decays. Furthermore, once the absolute vorticity becomes positive and the vortex has entered a less intense regime, the peak vorticity necessarily decays.

4.3. Radius of maximum velocity

The shift of the radius of maximum velocity $R_{\max}$ results as a combination of radial diffusion (Kloosterziel [12]) and nonlinear Ekman effects (Kloosterziel and van Heijst [2]; Maas [4]; ZSvH [8]). The linear Ekman term does not play any role in this process. Lateral friction induces an outward shift of $R_{\max}$ in either cyclones and anticyclones, while nonlinear Ekman terms produce and outward shift for cyclones and inward for anticyclones. This implies that both effects are reinforced in the cyclonic case, while they are opposed in the anticyclonic vortex.

As in the case of the peak vorticity, the simulation for the strong anticyclone shows that nonlinear Ekman effects are dominant at early stages of motion (when $R_{\max}$ decreases), while lateral friction becomes more

important at later stages (when R_{max} increases). This is not surprising since the Ekman suction is reduced as the anticyclone decays, i.e. for lower vorticity values.

5. Summary

By means of numerical simulations based on the 2D formulation (1), it has been shown that the viscous decay of cyclonic and anticyclonic non-isolated vortices is asymmetric due to the presence of nonlinear Ekman effects. The main differences are the faster decay of cyclones compared with anticyclones (Kloosterziel and van Heijst [2]) and radial advection of fluid, outward in cyclones, and inward in anticyclones (Maas [4]). In the conventional 2D formulation (6), where only the linear Ekman term is present, none of these effects are observed (see also ZSvH [8]).

The radial motion of fluid particles takes place in a spiral fashion. This motion is derived from the fact that, according to the Ekman condition, the radial and the azimuthal velocities are proportional, see (12). In cyclonic vortices fluid is pumped from the Ekman layer, thus producing the radially outward advection; the opposite process occurs in anticyclones, where there is suction from the vortex into the boundary layer, therefore inducing the inward advection of fluid. Both features are captured by the simple 2D viscous model (1) remarkably well.

The difference in the decay of cyclones and anticyclones is a consequence of the radial advection of fluid. Recall that both types of vortices are damped by the main contribution of bottom friction, namely by linear Ekman effects (stretching and squeezing effects). In cyclonic vortices, an additional amount of kinetic energy is lost when fluid is radially removed outward, while the total angular momentum is nearly conserved. This assumption seems reasonable since viscous effects are relatively weak (low Ekman number). The radius of maximum velocity increases due to lateral friction (Kloosterziel [12]) and the radial advection of fluid, both of them acting radially outward. The maximum velocity, energy and peak vorticity decay monotonically.

In contrast, anticyclones present a more complicated behaviour as fluid is advected inward, due to the Ekman layer. For the case of weak anticyclones, the loss of kinetic energy is lower than in cyclones, since the inward motion implies a lower decrease of the azimuthal velocity, according to the absolute angular momentum considerations. For strong anticyclones the opposite situation may occur, i.e. the azimuthal velocity may be increased as the fluid moves inward. The net result (taking into account the linear damping and lateral viscosity), however, is the decay of the vortex. At initial stages of motion a decrease of the radius of maximum velocity and an increase of the peak vorticity is observed. This is due to the relative importance of nonlinear Ekman effects when the vortex is still intense, and therefore the Ekman suction becomes more relevant. In general, it can be concluded that the additional source of energy for anticyclones, which makes them decay slower than cyclones, is provided by the spiral inward motion of fluid associated with the Ekman layer circulation, while nearly conserving total angular momentum.

Acknowledgments

References

[1] Hopfinger E.J., van Heijst G.J.F., Vortices in rotating fluids, Annu. Rev. Fluid Mech. 25 (1993) 241–289.

[2] Kloosterziel R.C., van Heijst G.J.F., The evolution of stable barotropic vortices in a rotating free-surface fluid, J. Fluid Mech. 239 (1992) 607–629.

[3] Kloosterziel R.C., van Heijst G.J.F., An experimental study of unstable barotropic vortices in a rotating fluid, J. Fluid Mech. 223 (1991) 1–24.

[4] Maas L.R., Nonlinear and free-surface effects on the spin-down of barotropic axisymmetric vortices, J. Fluid Mech. 246 (1993) 117–141.

[5] Sipp D., Lauga E., Jacquin L., Vortices in rotating systems: Centrifugal, elliptic and hyperbolic type instabilities, Phys. Fluids 11 (1999) 3716–3728.

[6] Gill A.E., Atmosphere-Ocean Dynamics, Academic Press, 1982.

[7] Pedlosky J., Geophysical Fluid Dynamics, Springer-Verlag, New York, 1987.

[8] Zavala Sansón L., van Heijst G.J.F., Nonlinear Ekman effects in rotating barotropic flows, J. Fluid Mech. 412 (2000) 75–91.

[9] Zavala Sansón L., van Heijst G.J.F., Backx N.A., Ekman decay of a dipolar vortex in a rotating fluid, Phys. Fluids 13 (2001) 440–451.

[10] van Heijst G.J.F., Kloosterziel R.C., Williams C.W.M., Laboratory experiments on the tripolar vortex in a rotating fluid, J. Fluid Mech. 225 (1991) 301–331.

[11] Orlandi P., Carnevale G.F., Evolution of isolated vortices in a rotating fluid of finite depth, J. Fluid Mech. 381 (1999) 239–269.

[12] Kloosterziel R.C., On the large-time asymptotics of the diffusion equation on infinite domains, J. Eng. Maths. 24 (1990) 213–236.